Journal of Hazardous Materials 186 (2011) 1007–1017

Contents lists available at ScienceDirect

Journal of Hazardous Materials

journal homepage: www.elsevier.com/locate/jhazmat

Factorial design analysis for sorption of zinc on hydroxyapatite

S. Meski*, S. Ziani, H. Khireddine, S. Boudboub, S. Zaidi

Faculté de Technologie, Département de Génie des Procédés, Laboratoire de Génie de l'Environnement, Université de Bejaia, Algeria

ARTICLE INFO

Article history:
Received 15 July 2010
Received in revised form
19 November 2010
Accepted 23 November 2010
Available online 30 November 2010

Keywords:
Adsorption
Statistical modeling
Hydroxyapatite
Zinc
Precipitation

ABSTRACT

A factorial design was employed to evaluate the quantitative removal of zinc from aqueous solutions on synthesized hydroxyapatite. The experimental factors and their respective levels studied were the initial zinc concentration in solution ($35 \leq C_{Zn} \leq 85$ mg/L), adsorbent dosage ($4.5 \leq C_{susp} \leq 9.5$ g/L), Ca/P molar ratio ($1.667 \leq Ca/P \leq 2$) and calcination temperature of hydroxyapatite ($600 \leq T_{Cal} \leq 800$ °C). The adsorption parameters were analysed statistically by means of variance analysis by using the STATISTICA software.

The experimental results and statistical analysis show that increasing in the calcination temperature from 600 to 800 °C decrease the zinc adsorption whereas the increase of adsorbent dosage increases it. Based on the analysis of variance and the factorial design of experiments, adsorbent dosage has a positive effect on the removal of zinc, whereas zinc concentration, Ca/P molar ratio and calcination temperature have a negative effect on this process. The factorial results also demonstrate the existence of statistically significant binary interactions of the experimental factors. The experimental results were fitted to the Langmuir and Freundlich equations to find out adsorption capacities. In most cases, the results indicate that the sorption data fits well in the Freundlich isotherm model.

The results of XRD analysis, pH_{PZC} and pH_{Final} values indicated that ion exchange and dissolution/precipitation mechanisms predominate for the sorption of zinc on our hydroxyapatite.

1. Introduction

Industrial wastewater contaminated with heavy metals is commonly produced from many kinds of industrial processes [1–3]. Therefore, if this wastewater is not treated with a suitable process or leaked from storage tanks, it can cause a serious environmental problem in the natural eco-system.

Whenever toxic heavy metals are exposed to the natural ecosystem, accumulation of metal ions such as lead, cadmium, zinc and mercury in human body will occur through either direct intake or food chains [4]. Therefore, heavy metal should be prevented before it reaches to the natural environments because of its toxicity.

Many treatment processes have been applied for the removal of heavy metals from wastewater such as: adsorption [5], chemical precipitation [6], ion exchange [7], reverse osmosis [8], ion flotation [9], and electrochemical treatment [10]. Among the various water-treatment techniques described, adsorption is generally preferred for the removal of heavy metal ions due to its high efficiency, easy handling, availability of different adsorbents and cost effectiveness [11,12].

Hydroxyapatite (HAP) is an efficient adsorbent and its high capacity in Zn immobilization has been reported [13–15]. Many researchers have assessed its dissolution [16], crystallinity [17], surface activity and thermal stability [18].

The influence of several operating parameters, such as initial metal concentration, temperature, pH and adsorbent dosage were investigated in batch mode. The published information in literature about adsorption of zinc in hydroxyapatite is well detailed [13–15,19]. The conventional and classical methods of studying a process by maintaining other factors involved at an unspecified constant level does not depict the combined effect of all the factors involved. The conventional technique for the optimization of a multivariable system usually defines one-factor at a time. Such a technique needs to perform a lot of experiments and could not reveal the alternative effects between components. This method is also time consuming and requires a number of experiments to determine optimum levels, which are unreliable.

Recently many statistical experimental design methods have been employed in chemical process optimization. Experimental design technique is a very useful tool for this purpose as it provides statistical models, which help in understanding the interactions among the parameters that have been optimized [20–23]. These methods involve mathematical models for designing chemical processes and analysing the process results. Among them, a 2^K factorial design methodology is one suitable method utilized in many fields.

* Corresponding author.
E-mail addresses: meskisamira@yahoo.fr (S. Meski), zamilas80@hotmail.com (S. Ziani), khiredine.hafit@gmail.com (H. Khireddine).

0304-3894/$ – see front matter © 2010 Elsevier B.V. All rights reserved.
doi:10.1016/j.jhazmat.2010.11.087

Table 1
Values of operating variables used in the designed set of experiments.

Operating variables	−1	0	1
x_1 zinc concentration (mg/L)	35	60	85
x_2 adsorbent dosage (g/L)	4.5	7	9.5
x_3 Ca/P molar ratio (Initial)	1.667	1.833	2
x_3 Ca/P molar ratio (Final)	1.616	1.852	2.161
x_4 calcination temperature of the hydroxyapatite (°C)	600	700	800

The present paper reports the results of a study of the sorption of zinc from aqueous solution onto hydroxyapatite. The effects of the operating parameters, such as initial zinc concentration (C_{Zn}), adsorbent dosage (C_{susp}), molar ratio Ca/P and calcination temperature of the hydroxyapatite (T_{cal}) on the adsorption of zinc were investigated. The main objective of this paper was to examine the main effect of the parameters considered and their interactions.

2. Experimental

2.1. Materials

All the reagents used were of analytical grade chemicals. A stock solution of zinc ions was prepared by dissolving appropriate amount of $ZnSO_4{\cdot}7H_2O$ (Aldrich Chemical Company, USA) in distilled water

2.2. Preparation of the adsorbent

The powders of hydroxyapatite were prepared by a conventional aqueous precipitation method from the addition of a diammonium phosphate solution $(NH_4)_2HPO_4$ (98% purity) into a reactor containing a calcium nitrate solution $(Ca(NO_3)_2, 4H_2O$, 98% purity). The pH of the solution was maintained at a constant value (pH ≈ 11) by the addition of an ammonium hydroxide solution using a pH stat (HANNA Instruments). The suspension was continuously stirred. After total addition of $(NH_4)_2HPO_4$ solution, the suspension was matured during 72 h. Then, it was filtered without washing. The resulting precipitate was dried at 80 °C. Synthesis conditions (i.e., Ca/P molar ratio of initial reagents) were adjusted in order to synthesis powders with variable Ca/P molar ratio. The purity of the initial powders used to prepare the reagent solutions was controlled. This parameter is taken into account in the calculation of the concentrations of reagents solutions.

The calcination was performed in the following heating schedule: 10 °C/min up to the desired temperature (600 °C, 800 °C and 700 °C), and a plateau with a residence time at this temperature of 3 h. Then, it was cooled down at 10 °C/min to room temperature

2.3. Characterization of the adsorbent

The simultaneous thermogravimetric analysis (TG) and differential thermal analysis (DTG) of the powders were performed (SETARAM TG-DTA92) in nitrogen atmosphere from room temperature to 800 °C at a heating rate of 10 °C/min. To study the crystallinity of the prepared samples, powder X-ray diffraction (XRD model PHILIPS X pert prof, analytical, system MPD) patterns were recorded using CuKα radiation at 50 kV and 100 mA. Fourier transform infrared spectrophotometry (SHIMADZU-8300 IR-TF) analysis was performed to identify the presence of functional groups in the samples. The results were plotted using the ORIGIN-6 software.

2.4. Batch mode studies

The stock solution was diluted as required to obtain standard solutions containing 35–85 mg/L of Zn(II). A volume of 200 mL of Zn(II) solution of a desired concentration, adjusted to a desired pH (pH 5), was taken in reaction bottles of 400 mL capacity and known amounts of adsorbents were added. The solution pHs was adjusted by using 0.1N nitric acid or dilute sodium hydroxide solutions. The suspensions were agitated for 2 h at 20 ± 1 °C in a shaking incubator. The suspension was filtered and the final concentration of Zn^{2+} in solution was measured by using the atomic absorption spectrophotometry technique (SHIMADZU AA 6500, air/C_2H_2 gas mixture).

The contact time, temperature and pH were fixed at their optimum value on the basis of the results of preliminary tests performed to study the effect of these parameters on the adsorption of zinc by hydroxyapatite.

2.5. Statistical method

2^K factorial designs are widely used in experiments involving several factors, where it is necessary to study the joint effect of the factors on a response. The most important of these cases is that of the k factors each at only two levels (minimum and maximum). A complete replicate of such a design requires 2^K observations and is called 2^K factorial design. 2^K factorial design allows the performance of an analysis of variance and the fitting of a response surface [24].

Table 2
Experimental results of 2^4 designs for the break-though time.

N	Coded experiments matrix				Experimental plan				Measured response
	C_{Zn} (mg/L)	C_{susp} (g/L)	Ca/P	T_{cal} (°C)	C_{Zn} (mg/L)	C_{susp} (g/L)	Ca/P	T_{cal} (°C)	Y (%)
01	−1	−1	−1	−1	35	4.5	1.667	600	85.037
02	−1	−1	−1	+1	35	4.5	1.667	800	82.068
03	−1	−1	+1	−1	35	4.5	2	600	84.516
04	−1	−1	+1	+1	35	4.5	2	800	65.866
05	−1	+1	−1	−1	35	9.5	1.667	600	84.374
06	−1	+1	−1	+1	35	9.5	1.667	800	85.549
07	−1	+1	+1	−1	35	9.5	2	600	88.134
08	−1	+1	+1	+1	35	9.5	2	800	89.725
09	+1	−1	−1	−1	85	4.5	1.667	600	88.839
10	+1	−1	−1	+1	85	4.5	1.667	800	73.875
11	+1	−1	+1	−1	85	4.5	2	600	83.551
12	+1	−1	+1	+1	85	4.5	2	800	76.598
13	+1	+1	−1	−1	85	9.5	1.667	600	89.649
14	+1	+1	−1	+1	85	9.5	1.667	800	76.148
15	+1	+1	+1	−1	85	9.5	2	600	79.230
16	+1	+1	+1	+1	85	9.5	2	800	79.073

It provides the smallest number of runs with which k factors can be studied in a complete factorial design. Because there are only two levels for each factor, it is assumed that the response is approximately linear over the range of the factor levels chosen [24,25].

The experimental results (behavior of the system) of 2^K factorial design can be easily expressed in terms of a regression model response explained by the following first degree polynomial Eq. (1):

$$Y_{\text{predicted}} = b_0 + \sum_{i=1}^{n} b_i x_i + \sum_{i=1}^{n}\sum_{j=1}^{n} b_{ij} x_i x_j \quad (1)$$

With four factors, 2^4 factorial designs require 16 runs. Meanwhile, the number of coefficients of $b_{i,i} = 0 \ldots 16$ to be estimated is 16.

Where, $Y_{\text{predicted}}$ represents the zinc adsorption yield, b_0 is the value of fitted response at the center point of design, b_i and b_{ij} are the linear interaction and quadratic terms, respectively.

According to practical experiences carried out the following four process parameters: initial zinc concentration (C_{Zn}) – factor 1 (x_1), adsorbent dosage (C_{susp}) – factor 2 (x_2), Ca/P molar ratio – factor 3 (x_3) and calcination temperature (T_{Cal}) – factor 4 (x_4) were foreseen as affecting the zinc removal. Minimum and maximum levels of each influential factor are reported in Table 1.

The response variable in this study is the sorption yield of zinc calculated as follows:

$$\%Y_{\text{exp}} = \frac{C_{(Zn)0} - C_{(Zn)e}}{C_{(Zn)0}} \times 100 \quad (2)$$

where $C_{(Zn)0}$ and $C_{(Zn)e}$ are initial and equilibrium concentration (mg/L).

3. Results and discussion

3.1. Thermogravimetric analysis

The DTG and TG curves for the hydroxyapatite powders after drying are illustrated in Fig. 1. The first endothermic region range from 30 to 110 °C with a peak at about 70 °C, which corresponds to the loss of physically adsorbed water molecules of the two hydroxyapatite powders. The weight loss in this region is 4% for hydroxyapatite with molar ratio (Ca/P = 1.667) and 6.5% for hydroxyapatite with the molar ratio (Ca/P = 2). With increasing temperature from 110 °C to 250 °C, small peak at about 200 °C has been observed in the two powders and a weight loss of 0.85% (for Ca/P = 1.667) and 3.95% (for Ca/P = 2) are observed at the TG curve in the temperature range which corresponds to loss of chemisorbed water. A third endothermic region ranges from 250 °C to 400 °C, which corresponds to the loss of the chemisorbed water.

The weight loss in the temperature range from 400 °C to 800 °C was 1.5% (for Ca/P = 2) and 0.65% (for Ca/P = 1.667), this corresponds to water loss from HPO_4^{2-} and a loss from CO_3^{2-} decomposition on heating to 800 °C and the remainder of water that is more strongly held by the crystals than the chemisorbed layer. The water loss from HPO_4^{2-} can be explained by the following reaction [26]:

$$2HPO_4^{2-} \rightarrow P_2O_7^{4-} + H_2O \quad (3)$$

$$P_2O_7^{4-} + 2OH^- \rightarrow 2PO_4^{3-} + H_2O \quad (4)$$

3.2. FTIR analysis

The FTIR spectrum Fig. 2(a) and (b) shows a number of absorption peaks, indicating the complex nature of hydroxyapatite. Bands of HAP [27]: (a) the bands at 3572 cm^{-1} and 631 cm^{-1} arise from stretching, librational, and translational modes, respectively, of OH^- ions; (b) The 1113 cm^{-1} and about 1040 cm^{-1} bands arise from ν_3 PO_4^{3-}, the 614 cm^{-1} band arises from ν_4 PO_4^{3-}, and the 474 cm^{-1} band arises from ν_2 PO_4^{3-} [28]. Bands in the 1180–1200 cm^{-1} region derive from HPO_4^{2-}, were not detected because of their weak intensities and are obscured by the PO_4^{3-} bands at 1113–1040 cm^{-1} [29]. The band at 875 cm^{-1} is attributed to arise from HPO_4^{2-} ions. In addition, this 875 cm^{-1} HPO_4 band was, as expected, missing in spectra of the powders that had been heated at different temperatures because of condensation of HPO_4^{2-} ions to form $P_2O_7^{4-}$ ions and H_2O [26]. (c) The group of weak intensity bands in the 2250 cm^{-1} to 1950 cm^{-1} region derives from overtones and combinations of the ν_3 and ν_1 PO_4^{3-} modes. Bands of CO_3^{2-} impurity ions: The bands at about 1410 cm^{-1} is attributed to components of the ν_3 mode of CO_3^{2-} groups that are the result of the dissolution of $CO_{2(g)}$ in the reaction solution. The diminution of the intensity of the carbonate bands in the powders heated at different temperatures can be explained by the decomposition of the carbonate at the high temperature. These results confirm those obtained by the TG analysis.

Bands of H_2O molecules: The broad band from about 3700 cm^{-1} to 2500 cm^{-1} derives from the ν_3 and ν_1 stretching modes of hydrogen-bonded H_2O molecules, and the band at 1630 cm^{-1} derives from the OH group in the hydroxyapatite structure [13].

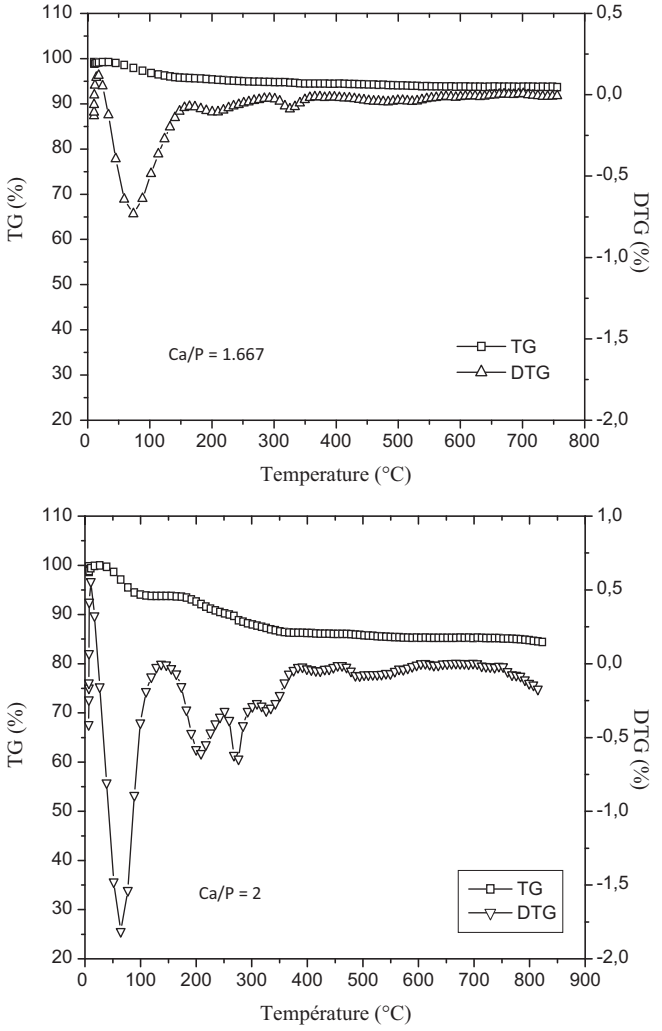

Fig. 1. TG and DTG pattern of the different Ca/P molar ratios hydroxyapatite powder under nitrogen atmosphere.

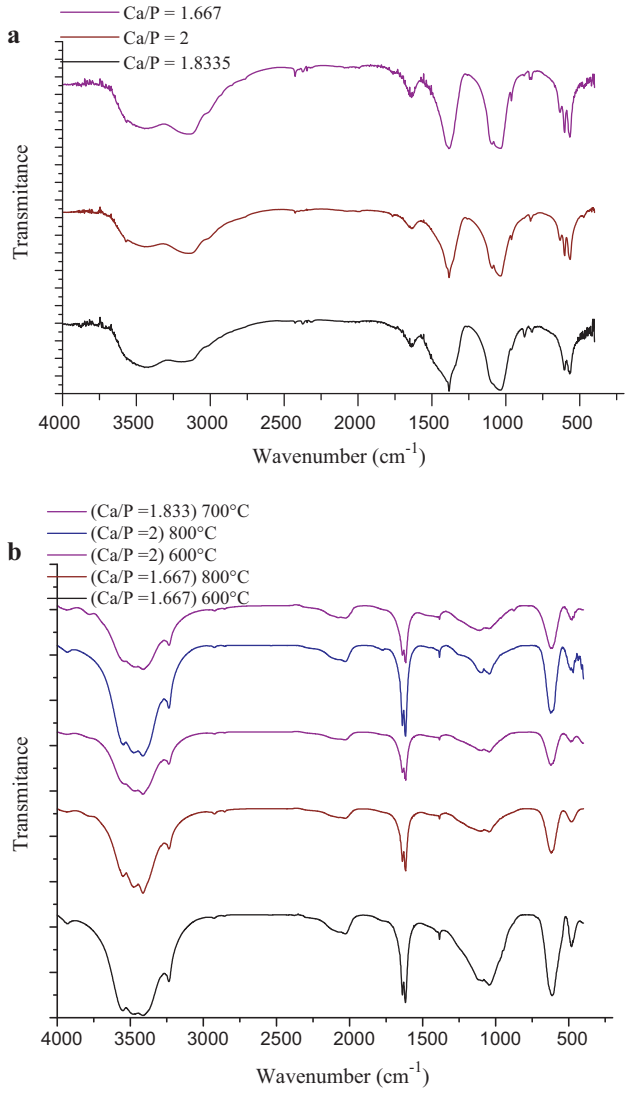

Fig. 2. IR spectra of powders (a) before and (b) after thermal treatment.

3.3. XRD phase analysis

Fig. 3 represents the XRD pattern of the synthesized hydroxyapatite powders. It reveals the presence of nanocrystalline apatite in the powders. As the annealing temperature increased to 600 °C and 800 °C, the intensity of apatite-characterized peaks gradually increased indicating an increase in crystallinity and crystalline size of particles. The XRD peaks obtained for the hydroxyapatite (Ca/P = 1.667) and (Ca/P = 2) samples are having strong agreement with the characteristic peaks of HAP pattern [13,28]. For Ca/P = 1.8335 and 2, the excess calcium was difficult to characterize. Nevertheless, CaO could be detected in the both powders (Ca/P = 1.8335 (calcined at 700 °C) and Ca/P = 2 (calcined at 600 °C)) indicating that the as synthesized powders should be constituted of HAP and $Ca(OH)_2$ which is the stable form of CaO at room temperature [30]

3.4. Experimental design and analysis statistic

Experimental results obtained in the sorption runs are presented in Table 2. A linear model, given by Eq. (5), was used for preliminary regression fits (STATISTICA software). Linear interaction and quadratic effects of the factors (in the coded levels x_1, x_2, x_3 and x_4, see Table 2) were considered in this model. Coefficients of the respective effect were represented by b_i.

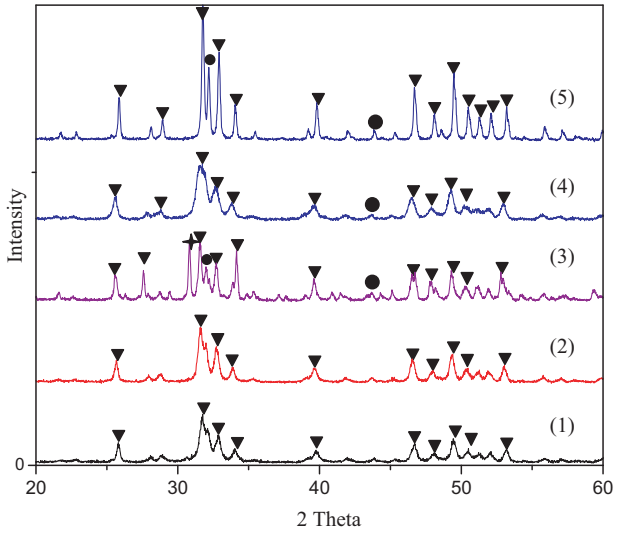

Fig. 3. XRD patterns of as synthesized powders. Triangle: hydroxyapatite, circle: CaO and Stars: $CaCO_3{\cdot}O_{65}{\cdot}H_2O$. (1) and (2): Ca/P = 1.667, T = 600 °C and 800 °C respectively, (3) and (4): Ca/P = 2, T = 600 and 800 °C respectively and (5): Ca/P = 1.83 and T = 700 °C.

$$\begin{aligned} Y_{\text{predicted}} = {} & b_0 + b_1x_1 + b_2x_2 + b_3x_3 + b_4x_4 + b_{12}x_1x_2 + b_{13}x_1x_3 \\ & + b_{14}x_1x_4 + b_{23}x_2x_3 + b_{24}x_2x_4 + b_{34}x_3x_4 \\ & + b_{123}x_1x_2x_3 + b_{124}x_1x_2x_4 + b_{134}x_1x_3x_4 \\ & + b_{234}x_2x_3x_4 + b_{1234}x_1x_2x_3x_4 \end{aligned} \quad (5)$$

The effect of each variable was determined as the difference between the average value of the response for the experiment at the high level (+) and the average value for the experiments at the low level (−), using the Yates algorithm [31].

$$E_I = \frac{\sum Y_{\text{exp}}(+)}{n} - \frac{\sum Y_{\text{exp}}(-)}{n} \quad (6)$$

where E_i is the effect of the variable, Y_{exp} the measured response, and n is the number of experiments at each level (− or +). The regression coefficients and the effects are shown in Table 3.

Table 3
Statistical parameters for 2^4 designs.

Factor	Coefficients	Effect	t_j	Significance
b_0	82.000	82.00	184.531	S
b_1	−1.14	−2.287	2.573	S
b_2	1.971	3.942	4.435	S
b_3	−1.178	−2.356	2.651	S
b_4	−3.402	−6.804	7.655	S
b_{12}	−1.82	1.654	4.086	S
b_{13}	−0.079	−4.644	0.178	NS
b_{14}	−1.044	−9.092	2.350	S
b_{23}	1.233	1.585	2.775	S
b_{24}	2.040	−2.862	4.591	S
b_{34}	0.380	−9.160	0.855	NS
b_{123}	−1.849	−4.401	4.161	S
b_{124}	−1.008	−7.166	2.268	S
b_{134}	2.289	−6.870	5.150	S
b_{234}	1.339	−2.539	3.014	S
b_{1234}	−0.673	−5.964	1.514	NS

NS: no significant.
S: significant.

Table 4
Experimental results of the center point of the experimental domain.

Essai No.	Y_0 (%)
1	90.39
2	90.60
3	91.09
4	92.41
5	89.69
6	86.36
7	90.60
8	93.22
9	91.09
10	92.41
11	92.21
12	91.1

In order to determine the significant effects on the response, Student's *t*-test was employed [32]. The effects determined as non-significant were then eliminated and a new fit was performed, resulting in a reduced model. The *t* value represents the ratio of the coefficient to the estimated parameter and standard deviation residual according the following equation:

$$t_j = \frac{|b_j|}{\sqrt{\left(\frac{1}{N}\right)\left(\frac{\sum_{1}^{m}(Y_{0I}-Y_{0\text{mean}})_2}{(m-1)}\right)}} \quad (7)$$

where b_j: coefficient; N: number of experiment ($N = 16$); m: number of experiment at the central point; Y_{0i}: observed value of adsorption yield at the i central point; $Y_{0\text{mean}}$: mean adsorption yield at the central point.

The experimental error was evaluated by 12 measurements at the center point of the experimental domain (Table 4).

It was observed that at 95% confidence level and 11 freedom degrees ($m-1$), the t_{crit}-value equal to 2.2. All effects (Table 3) presenting t higher than 2.2 have statically significance. It is found in Fig. 4, which illustrated the graphical representation of "size effect" of each of parameters upon the adsorption of zinc by the hydroxyapatite that all individual effects are significant at 5% of significance level. From this figure it can be seen that zinc concentration (x_1), molar ratio Ca/P (x_3) and calcination temperature of the hydroxyapatite (x_4) have a negative effect, while the adsorbent dosage (x_2) has a positive effect on the response. The interaction term C_{Zn}-Ca/P

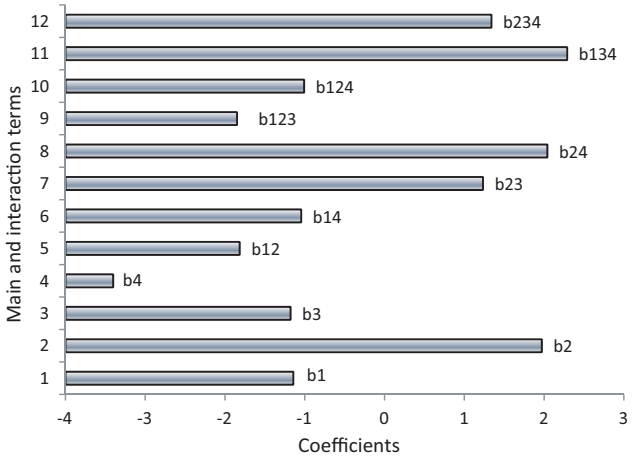

Fig. 4. The significant main and interaction terms of zinc adsorption.

Table 5
Analysis of variance-reduced model fit for zinc adsorption.

Factor	Degrees of freedom	SSE	SSR	SST	MSE
b_0	13	0.138	11.527	9.139	0.011
b_1	1	0.045	0.025	0.003	0.045
b_2	1	0.138	4.538	6.261	0.138
b_3	1	0.045	254.084	260.947	0.045
b_4	1	0.949	1.920	5.570	0.949
b_{12}	1	1.282	21.781	12.493	1.282
b_{14}	1	1.282	43.274	59.457	1.282
b_{23}	1	1.282	32.402	46.579	1.282
b_{24}	1	0.949	51.340	66.245	0.949
b_{123}	1	0.949	40.841	29.336	0.949
b_{124}	1	0.045	61.603	58.292	0.045
b_{134}	1	0.138	38.917	34.414	0.138
b_{234}	1	0.045	8.984	7.748	0.045

(coded x_1x_3), Ca/P-T_{cal} (coded x_3x_4) and C_{Zn}-C_{susp}-Ca/P-T_{cal} (coded $x_1x_2x_3x_4$) were no significant. Thus, a reduced model, represented by Eq. (8), was used to fit experimental data of zinc sorption by hydroxyapatite:

$$Y_{\text{predicted}} = 82 - 1.14x_1 + 1.971x_2 - 1.178x_3 - 3.402x_4 - 1.82x_1x_2 - 1.044x_1x_4 - 1.233x_2x_3 + 2.04x_2x_4 - 1.849x_1x_2x_3 - 1.008x_1x_2x_4 + 2.289x_1x_3x_4 + 1.339x_2x_3x_4 \quad (8)$$

3.5. Analysis of the variance (ANOVA)

After estimating the main effects, the interacting factors affecting the removal of zinc and the test of the significance, the adequacy of the regression were determined by performing the analysis of variance (ANOVA) [33]. Error functions were defined to determine the significance of each parameter in model, the parameter values, and to establish the fit of the model to the experimental data. The sum of the squared variation of the experimental sorption yield (Y_{exp}) and predicted yield ($Y_{\text{predicted}}$) to the mean experimental adsorption yield ($Y_{\text{exp,mean}}$) and the sum of the squared residual between experimental and predicted sorption values are the basis of this error analysis. The sum of squared total (SST), sum of squares for regression (SSR) and sum of squared errors (SSE) were computed from the zinc sorption as follows [34]:

$$\text{SST} = \sum_{i=1}^{n}(Y_{\text{exp}} - Y_{\text{mean}})^2 \quad (9)$$

$$\text{SSR} = \sum_{i=1}^{n}(Y_{\text{predicted}} - Y_{\text{mean}})^2 \quad (10)$$

$$\text{SSE} = \sum_{i=1}^{n}(Y_{\text{exp}} - Y_{\text{predicted}})^2 \quad (11)$$

The variance of the random errors between the fitted model and the observed data can be measured from the value of SSE averaged with the degree of freedom according to the following equation [34].

$$\text{MSE} = S_e^2 = \frac{\text{SSE}}{\text{degree of freedom}} \quad (12)$$

MSE: the mean-square-error.

The parameters of the model were determined by minimizing SSE. These parameters are shown in Table 5.

Additionally, we have calculated the *F*-ratios (F_0) – defined as the ratio of the mean-square-effect and the mean-square-error (Eq.

(13)) [20].

$$F = \frac{\mathrm{SSR}}{(l-1)} - \frac{\mathrm{SSE}}{N-1} \quad (13)$$

where l: number of the significance parameters

If the model is a good predictor of the experimental results, F-calculated should be greater than the tabulated value of the F-distribution obtained at a level of significance and a certain number degrees of freedom [20].

The F-ratios obtained for zinc sorption "$F = 16.43$" is clearly greater than the tabulated F(8.74 at 95% significance), then the model fit is adequate.

3.6. Correlation coefficients

The regression coefficient (R^2) (Eq. (14)), evaluates the correlation between the experimental data and the predicted responses.

$$R^2 = \frac{\mathrm{SSR}}{\mathrm{SST}} \quad (14)$$

The obtained R^2 suggest good adjustments to the experimental results since these indicate that 98.5% of the variability in the response could be explained by the model. Adjusted R^2 (Adj R^2) (Eq. (15)) is also a measure of goodness of a fit, but it's more suitable for comparing model with different numbers of independent variables. It corrects the R^2-value for the sample size and the number of terms in the model by using the degrees of freedom on its computation, so if there are many terms in a model and not very large sample size, adjusted R^2 may be visible smaller than R^2 [35]. Here, adjusted R^2 value (92.5%) was closer to the corresponding R^2 value.

$$\mathrm{Adj}R^2 = R^2 - (1-R^2)\frac{(l-1)}{(N-l)} \quad (15)$$

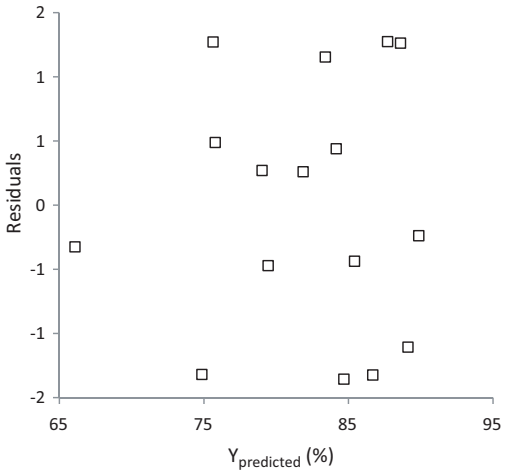

Fig. 5. Residuals versus predicted response for adsorption of zinc in the hydroxyapatite.

3.7. Residual analysis

In addition to these tests, the adequacy of the model was also evaluated by the residuals (difference between the experimental and the predicted values (Eq. (16))). Residuals are thought as elements of variation unexplained by the fitted model and then it is expected that they occur according to a normal distribution. The observed residuals are plotted against the predicted values (Fig. 5).

$$\mathrm{residual} = \varepsilon = \frac{(Y_{\mathrm{exp}} - Y_{\mathrm{predicted}}) \times 100}{Y_{\mathrm{exp}}} \quad (16)$$

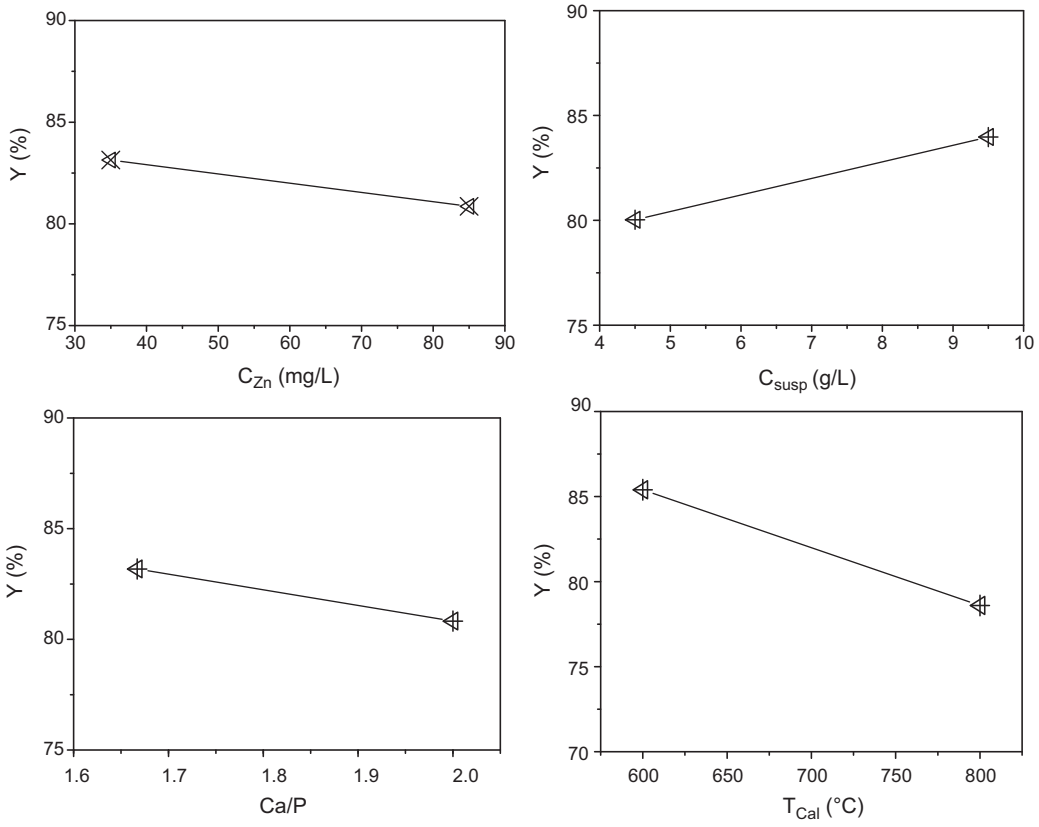

Fig. 6. Main effect plots.

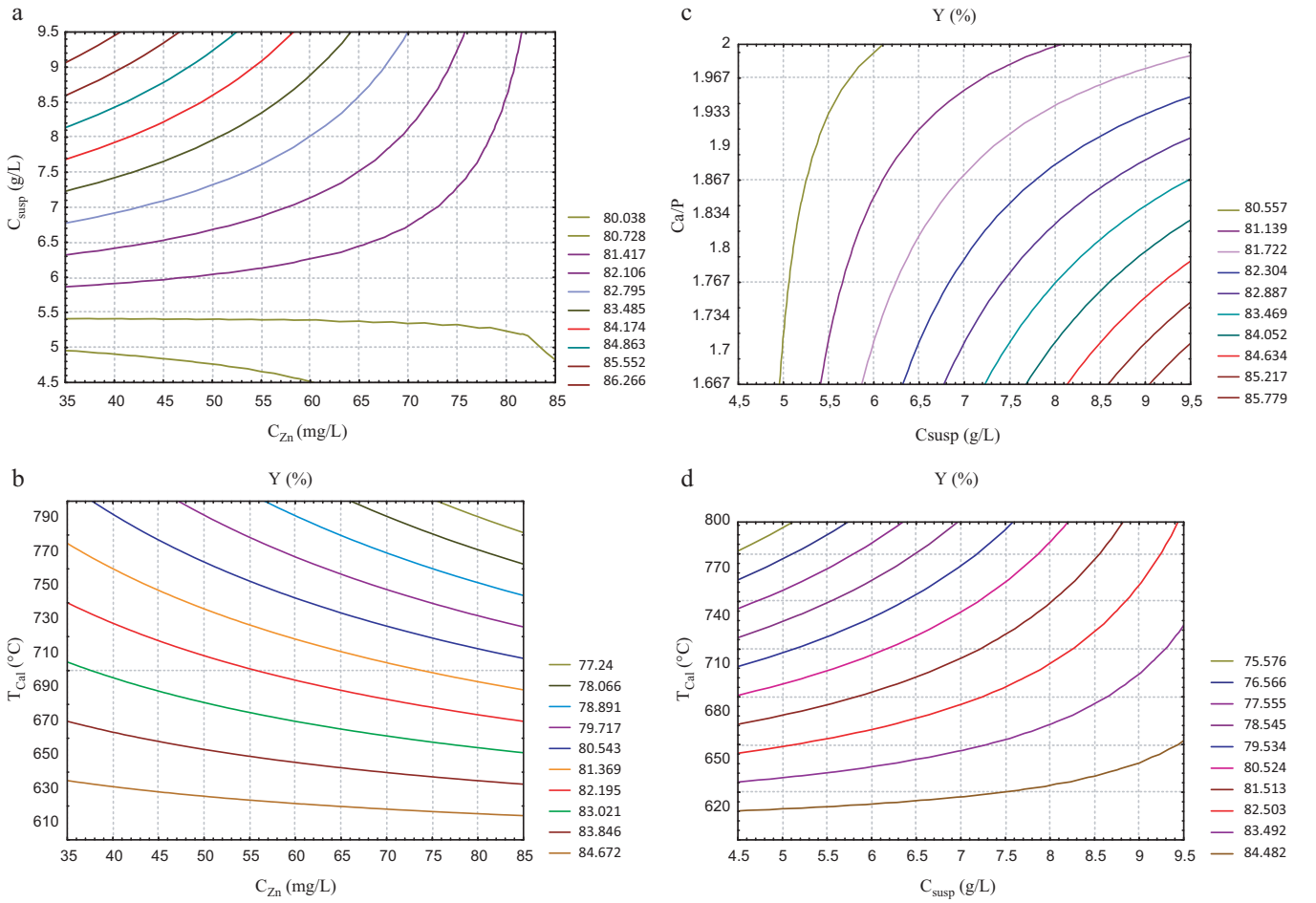

Fig. 7. Contour plots for interaction effects.

The plot of the residuals revealed that they have no obvious pattern and unusual structure. This implies that the model proposed is adequate and there is no reason to suspect any violation of the independence or constant variance assumption.

3.8. Main and interaction effects

The effect of each factor was statistically significant at $p < 0.05$ [24]. The main effects C_{Zn}, C_{susp}, Ca/P and T_{cal} and interactions effect of the process parameters were presented in Figs. 6 and 7 respectively. The sign of the main effect indicates the directions of the effect. It can be seen from Fig. 6, that the effect of T_{cal} was characterized by a greater degree of departure and also had a negative effect on the response, whereas, the concentration of the suspension has a positive effect on the response with greater departure. These expected observations are the result of the decrease of the surface area of the adsorbent. Decrease of the specific surface is due to the increase in the calcination temperature that causes the particle coalescence and densification of the hydroxyapatite [36], whereas the increase of the adsorption yield with the adsorbent dosage is related to the increase of the active site number [13]. On the other hand the percentage adsorption of zinc ions to the hydroxyapatite decreased as the initial concentration of metal ions was increased from 35 to 85 mg/L. This appears to be due to the increase in the number of ions competing for the available binding sites in the HAP. At lower concentrations, all metal ions present in solution could interact with the binding sites and thus determined 83% of adsorption at 35 mg/L concentration. At higher concentration, more zinc ions are left unadsorbed in solution due to the saturation of adsorption sites.

Contour plot is the projection of the response surface as a two dimensional plane. This analysis gives a better understanding of the influence of variables and their interaction on the response. Contour plot for the significance interactions were shown in Fig. 7. The interaction plots showed that interaction of C_{Zn} and C_{susp} played major role and also these two factors interacted strongly with other factors indicating predominance in the removal.

In Fig. 7(a) and (b) it can be observed that for high initial concentration of zinc values, an increase in adsorbent dosage and the decrease of calcination temperature respectively favors adsorption process. A relatively strong interaction existed between the adsorbent dosage and calcinations temperature (Fig. 7(d)). This interaction confirms the effect of adsorbent dosage and calcination temperature obtained on the interaction (a) and (b).

Fig. 7(c) shows that at constant conditions of initial concentration and calcination temperature, an increase in Ca/P between 1.667 and 2 causes a decrease of adsorption yield of zinc. This result can be due to the existence of the deficient cation (lacune) in the HAP with molar ratio Ca/P = 1.667, which can be compensated by zinc ions in order to obtain a stoichiometric apatite (than decrease of surface contact (adsorption site)). These results are similar to the earlier reported work in the literature. In the study by Baillez et al. [37] on the adsorption of lead by three different HAP powders (HAP_1(Ca/P = 1.6, specific surface area SSA = 41 m^2/g), HAP_2 (Ca/P = 1.67, SSA = 50 m^2/g)

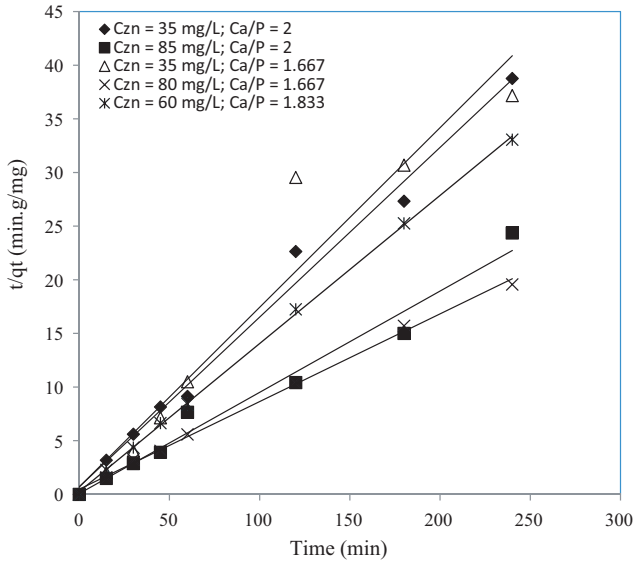

Fig. 8. Linearization of zinc sorption kinetics by hydroxyapatite: pseudo-second-order rate at different experimental conditions (Ca/P = 1.667 and 2 at T_{cal} = 600 °C and Ca/P = 1.833 at T_{cal} = 700 °C).

and HAP_3 (Ca/P = 1.73, SSA = 104 m^2/g)) it has been reported that HAP_1 and HAP_2 have same specific surface areas, but HAP_1 has the higher adsorption capacity (q_{max} = 450 mg/g (for HAP_1), 330 mg/g (HAP_2) and 360 mg/g (for HAP_3), then they conclude that the cation deficiency of the deficient HAP_1 (Ca/P = 1.6) can be compensated by lead ions in order to obtain stoichiometric apatite.

In our study the final Ca/P ratio is slightly different to the initial Ca/P ratio (Table 1). The precision was Ca/P = 1.667 ± 0.05. This result is confirmed by the existence of the band HPO_4^{2-} in the IR spectra, which was considered as the characteristic of calcium deficient hydroxyapatite by other researchers [38]. Difference between initial and final Ca/P ratio can be explained by: (1) stoichiometric defect of raw materials as chemical purity, water adsorption, etc.; (2) a slight variation of manufacturing process parameters, as working temperature, reaction pH, slurry stirring, weighing, etc.

3.9. Kinetics study

According to literature, several models can be used to express the kinetics of the sorption processes (e.g. first-order, pseudo-first, pseudo-second-order reaction model) [39]. The studies on the kinetics of the various sorption processes have revealed that over a long period of time pseudo-second-order model provides the best correlation [39]. Pseudo-second-order reaction model was applied to our experimental data in order to determine the sorption rate constant, at room temperature. The linear form of pseudo-second-order rate expression is:

$$\frac{t}{q_t} = \frac{1}{K_2 q_e^2} + \frac{1}{q_e} t \tag{17}$$

where q_e and q_t are the amounts of solute sorbed at equilibrium and time t (mg/g), K_2 is the equilibrium rate constant of pseudo-second-order (g/mg min). The following expression denotes the initial sorption rate h (mg/g min):

$$h = K_2 q_e^2 \tag{18}$$

The application of the linear form of pseudo-second-order kinetic model on our experimental results is presented in Fig. 8. Both constants K_2 and h were calculated from the intercept and slope of the line obtained by plotting t/q_t against t. The value of pseudo-second-order rate constant K_2, experimentally obtained amounts of solute sorbed at equilibrium and the values of initial sorption rate h are presented in Table 6.

Excellent agreement exists between the model and our experimental results ($0.931 \le R^2 \le 0.999$). Furthermore, theoretically predicted equilibrium sorption is close to that determined experimentally. The same kinetic model was used to define the sorption kinetics of metal cations on different apatites: Zn^{2+} on natural apatite derived from animal bones [13] and Pb^{2+} on hydroxyapatite prepared from egg shell [40].

3.10. Adsorption isotherms

The adsorption isotherms were used to determine the affinity of hydroxyapatite to zinc. The zinc concentration at equilibrium C_e was used to calculate the amount of zinc q_e (mg Zn^{2+}/g HAP) removed by a unit weight of hydroxyapatite at the end of the experiment. This quantity was defined as follows:

$$q_e = \frac{(C_0 - C_e)\, V}{m} \tag{19}$$

where C_o is the initial concentration of zinc (mg/L), C_e is the equilibrium concentration of zinc (mg/L), V is, the volume of the solution (L) and m is the weight of hydroxyapatite (g).

The adsorption isotherms of zinc adsorption on hydroxyapatite were depicted in Fig. 9.

According to the shapes of the curves (Fig. 9), the isotherm corresponding to zinc adsorption onto HAP with molar ratio (Ca/P = 1.667) and adsorbent dosage (C_{susp} = 9.5 g/L), may be classified as S type of the Giles classification [41]. This shape indicates that the adsorption becomes increasingly favored as concentration rises and is usually ascribed to strong competition with the solvent molecules for substrate sites. However the isotherms corresponding to zinc adsorption onto hydroxyapatite with molar ratios (Ca/P = 1.667 and Ca/P = 2) and adsorbent dosage (C_{susp} = 4.5 g/L) may be considered as C type of the Gilles classification, this fact implying that low range of adsorption was observed at these conditions.

The isotherm for zinc adsorption onto hydroxyapatite with molar ratio (Ca/P = 2) and adsorbent dosage (C_{susp} = 9.5 g/L) may be classified as L type of Gilles classification, reflecting a relatively high affinity between zinc and adsorbent. This also indicates that no strong competition occurs for the adsorption sites between solvent molecules and adsorbate molecules.

The equilibrium data obtained for the adsorbent with different molar ratios were fitted in the Langmuir and Freundlich isotherm models [13]. The following expressions of a straight line were used, found by means of mathematical transformation of isotherms:

For Langmuir isotherm:

$$\frac{C_e}{q_e} = \frac{1}{q_m} C_e + \frac{1}{q_m K_L} \tag{20}$$

where C_e is the equilibrium concentration of the adsorbate (mg/L), q_e is the amount of adsorbate adsorbed per unit mass of adsorbent (mg/g), q_m and K_L are Langmuir constants related to adsorption capacity and rate of adsorption, respectively. These parameters were calculated from the slope and intercept of Langmuir plots of C_e/q_e versus C_e. The results were listed in Table 7.

For Freundlich isotherm:

$$\ln q_e = \ln K_F + \frac{1}{n} \ln C_e \tag{21}$$

where C_e is the equilibrium concentration of the adsorbate (mg/L), q_e is the amount of adsorbate adsorbed per unit mass of adsorbent (mg/g), K_F and n are Freundlich constants with n giving an indication of how favorable the adsorption process and K_F (L/mg) is

Table 6
Pseudo-second-order parameters for the adsorption of Zn^{2+} at different conditions.

Conditions	K_2 (min^{-1})	R^2	h (mg/g min)	$q_{e\,exp}$ (mg/g)	$q_{predicted}$ (mg/g)
C_{zn} = 35 mg/L, Ca/P = 2, C_{susp} = 4.5 g/L and T_{cal} = 600 °C	0.022	0.986	0.986	6.585	6.622
C_{zn} = 35 mg/L, Ca/P = 1.667, C_{susp} = 4.5 g/L and T_{cal} = 600 °C	0.039	0.931	1.213	6.625	6.097
C_{zn} = 85 mg/L, Ca/P = 2, C_{susp} = 4.5 g/L and T_{cal} = 600 °C	0.016	0.989	2.247	12.265	11.627
C_{zn} = 85 mg/L, Ca/P = 1.667, C_{susp} = 4.5 g/L and T_{cal} = 600 °C	0.019	0.997	2.127	11.140	12.345
C_{zn} = 60 mg/L, Ca/P = 1.833, C_{susp} = 7 g/L and T_{cal} = 700 °C	0.076	0.999	4.016	7.260	7.256

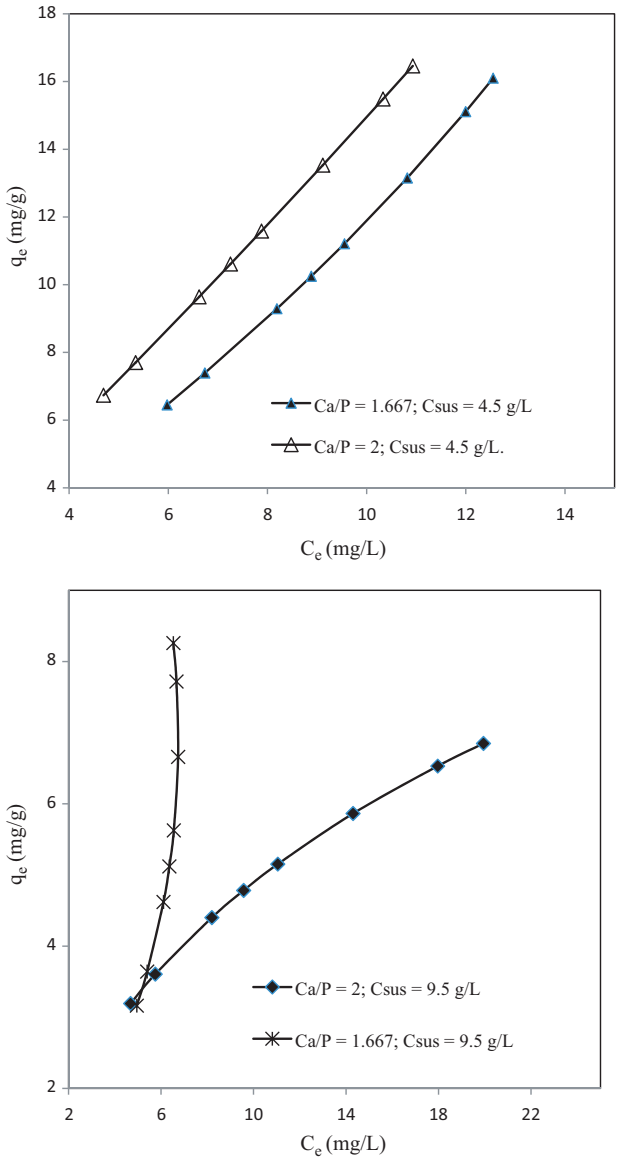

Fig. 9. Adsorption isotherms for zinc sorption on the four powders.

the adsorption capacity of the adsorbent. The parameters for the Freundlich model were listed in Table 7.

The analysis of results on the basis of the R^2 value for two isotherms equations shows that the data have agreed well with both the models, with the exception of the results obtained at (Ca/P = 1.667 and C_{susp} = 9.5 g/L). Therefore it can be inferred that just analysing the R^2 of the fitting is not the unique parameters that should be taken into account to verify the best fitting of isotherm model. However, from the Langmuir model, the determined slope is negative, thus it appears that this model is not favorable. These results are similar to earlier reported work in the literature. In the study by Ramnani and Sabharwal [42] on the adsorption of Cr(VI) onto radiation crosslinked chitosan it has been reported that the experimental data fits well in the Langmuir equation as a straight line plot is obtained. However the observed intercept is negative. Thus they concluded that Langmuir model does not imply in the adsorption of Cr(VI) on chitosan crosslinked by radiation.

Table 7
Isotherm parameters for different isotherms models.

Conditions		C_{susp} = 4.5 g/L		C_{susp} = 9.5 g/L	
		Ca/P = 1.667	Ca/P = 2	Ca/P = 1.667	Ca/P = 2
Langmuir	K_L ($L\,mg^{-1}$)	−0.020	−0.007	−0.106	0.086
	q_m (mg/g)	−45.45	−200	−2.697	10.752
	R^2	0.998	0.999	0.751	0.996
Freundlich	n	1.231	1.057	2.772	0.525
	K_F ($mg^{(1-1/n)}\,L^{1/n}\,g^{-1}$)	0.703	1.308	0.034	1.44
	R^2	0.988	0.999	0.818	0.998

3.11. Zinc removal mechanism

Sorption of zinc by hydroxyapatite was studied using the initial pH range 2–7. After 2 h of contact time, equilibrium pH (pH_{Final}) values were measured, as well as the residual metal concentrations and the results are presented in Fig. 10. In the same figure, the pH_{Final} versus $pH_{initial}$ plot, obtained by equilibrating hydroxyapatite powder with inert electrolyte (KCl) for pH_{PZC} determination, was also included. If no specific sorption from the solution occurs, acidic, as well as basic solutions (in the initial pH range 2–7) are buffered after the reaction with HAP to its pH_{PZC} value. The buffering characteristics of hydroxyapatite are the result of the acid–base reactions of the reactive surface sites.

According to Wu et al. [43], the reactions responsible for the surface properties of hydroxyapatite in aqueous solutions are:

$$\equiv PO^- + H^+ \Leftrightarrow POH^0 \quad (22)$$

$$\equiv CaOH_2^+ \Leftrightarrow CaOH^0 + H^+ \quad (23)$$

In the range of the lower initial pH values (below pH_{PZC} = 7.1) consumption of protons from the solution by the protonation of surface $\equiv PO^-$ and $\equiv CaOH^0$ groups results in a final pH increase. The positively charged $\equiv CaOH^{2+}$ and neutral $\equiv POH^0$ sites prevail on HAP surface in acidic solutions, making surface charge of

Table 8
Single-crystal size and crystallinity of HAP, Zn-HAP and Zn-HAP calcined at 600 °C.

Sample	Line width (2 1 3) FWHM (rad)	Average single-crystal size D (Å)	Crystallinity (X_c)
HAP	0.295	297	0.538
Zn-HAP	0.529	165	0.093
Zn-HAP calcined at 600 °C	0.446	196	0.155

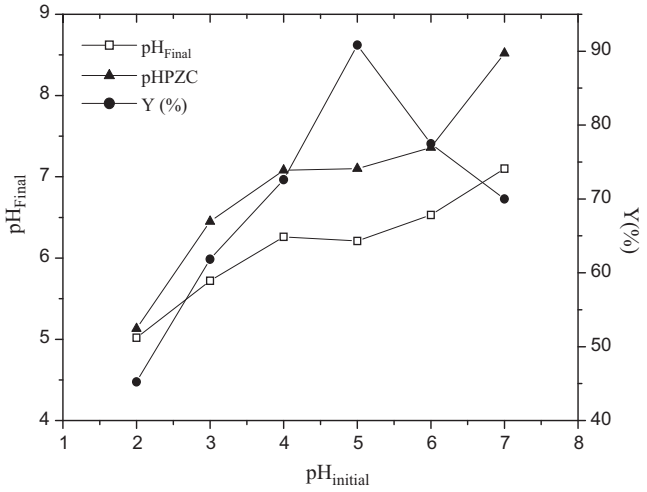

Fig. 10. Relationships between initial pH, final pH values obtained after equilibration of HAP with inert electrolyte (pH_{PZC}) and Zn^{2+} solution (pH_{Final}), and the yield of zinc sorbed.

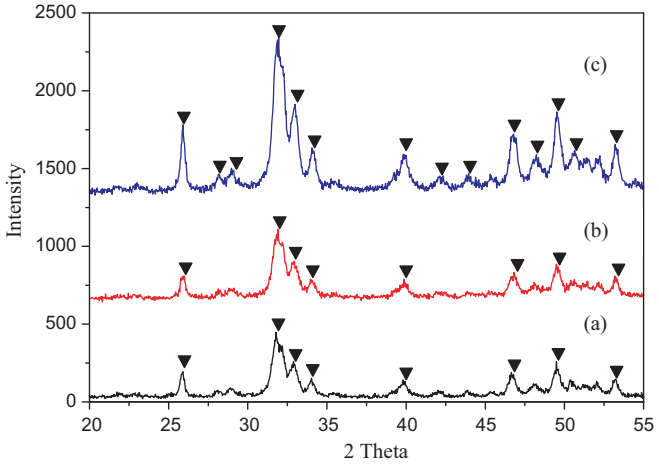

Fig. 11. Powder XRD patterns of the (a) hydroxyapatite no substituted, (b) Zn-substituted apatites and (c) Zn-substituted apatites heat-treated at 600 °C for 3 h.

hydroxyapatite in this pH region positive. The results showed that the removal efficiency of zinc increased significantly as the pH increased from 2 to 5 and decreased at pH range 5–7. Then the optimum pH for zinc sorption by HAP was found to be 5.

There are two possible reactions capable of removing zinc ion from the solutions. The first mechanism is the adsorption of Zn^{2+} on the surfaces followed by the ion exchange reaction between Zn^{2+}adsorbed and Ca^{2+} of HAP. The ion exchange interaction can be presented as follows [27,39]:

$$Ca_{10}(PO_4)_6OH_2 + xZn^{2+} \rightarrow Zn_xCa_{(10-x)}(PO_4)_6OH_2 + xCa^{2+} \quad (24)$$

The second mechanism is dissolution of HAP in aqueous solution containing zinc ions (which induced the increase on the pH_{Final}) followed by precipitation of zinc hydroxyapatite $Zn_{10}(PO_4)_6(OH)_2$, i.e., the dissolution-precipitation mechanism [27]. As low pH and the presence of Zn^{2+} ions both accelerate hydroxyapatite dissolution [44], released phosphates combine with Zn^{2+} ions to form the less soluble Zn-hydroxyapatite. This dissolution/precipitation mechanism is expressed as:

$$\text{Dissolution}: Ca_{10}(PO_4)_6OH_2 + 14H^+ \rightarrow 10Ca^{2+} + 6H_2PO_4^- + + 2H_2O \quad (25)$$

$$\text{Precipitation}: 10Zn^{2+} + 6H_2PO_4^- + 2H_2O \rightarrow Zn_{10}(PO_4)_6OH_2 + 14H^+ \quad (26)$$

In order to investigate the removal mechanism of Zn^{2+} ions by HAP in aqueous solution, X-ray diffraction patterns of the hydroxyapatite powder after immersing in 100 mg/L of Zn^{2+} solutions for 52 h are displayed in Fig. 11.

Phase analyses after exposure to a 100 mg/L Zn^{2+} solution showed no shift of the HAP peaks in XRD was found which would indicate an ion exchange in the hydroxyapatite structure.

On the other hand, the crystal size of the precipitates was estimated from the XRD pattern using the Scherrer equation [45]. According to this equation, a single-crystal dimension perpendicular to the ($h\,k\,l$) plane (D_{hkl}) can be estimated from the peak broadening as:

$$D_{hkl} = \frac{k\lambda}{B_{1/2}\cos\theta_{hkl}} \quad (27)$$

where k is a constant varying with the method of measuring the breadth and is chosen to be 0.9 for elongated HAP crystallites, λ is the wavelength (nm) of Cu K_α radiation ($\lambda = 0$, 15418 nm); $B_{1/2}$ corresponds to full width at half maximum (FWHM) for the peak $h\,k\,l$ (rad), θ_{hkl} is the diffraction angle (in degree). In samples with apatite structures, the line broadening of the (2 1 3) ($2\theta = 49.49$) reflection was used to evaluate the mean crystal size. The crystallinity degree, X_c, is defined as the fraction of the crystalline phase in a sample volume. An empirical relation between X_c and $B_{1/2}$ is commonly deduced according to the following equation [46]

$$X_c = \left(\frac{K_A}{B_{1/2}}\right)^3 \quad (28)$$

where K_A is a constant set at 0.24 and $B_{1/2}$ is the FWHM of the (2 1 3) reflection (in degrees). Table 8 shows the single-crystal size and crystallinity of HAP, Zn-HAP and Zn-HAP calcined at 600 °C.

The HAP crystallinity and crystallite size seem decrease after adsorption of zinc. This behavior might be explained by a mismatch in the ion size between Zn and Ca. Zn^{2+} ions (the ionic radius of Zn^{2+} is 0.074 nm, significantly smaller than that of Ca^{2+} (0.099 nm) [47]) might distort the crystal structure of HAP [48]. These results support the ion-exchange mechanism. However, the Zn-HAP calcined at 600 °C showed little increase on the crystallinity compared to the powder after adsorption. Our results are consistent with Miyaji et al.'s observation as they found that the crystallinity decreased with an increase in the Zn concentration [47]. LeGeros and LeGeros [49] reported that the incorporation of small amount of Zn^{2+} into the HAP structure induces an evident reduction in the degree of crystallinity of the apatitic phase, which leads to the inability of the structure to host greater amount of Zn.

4. Conclusions

The factorial design of experiments for batch adsorption of the zinc using hydroxyapatite was studied. The effects of four factors; initial zinc concentration (35–85 mg/L), adsorbent dosage (4.5–9.5 g/L), Ca/P molar ratio (1.667–2) and calcination temperature of the hydroxyapatite (600–800 °C) on percent of adsorption were identified. The statistical analysis for each case confirmed that the equation (Eq. (8)) gave a reasonably good fit with an R^2 value of 0.985. According to the significance effect obtained in variance analysis, the adsorbent dosage was found to have a significant effect on the adsorption of zinc and the molar ratio Ca/P and zinc concentration had a weak influence on the adsorption yield, except for the calcination temperature, which had a strong effect under the conditions investigated; the optimal adsorption yield is obtained

at a Ca/P ratio of 1.667. The increase in the adsorbent dosage has a positive effect on the removal of zinc and its optimal value is 9.5 g/L.

The kinetics of zinc sorption on hydroxyapatite is based on the assumption of the pseudo-second-order mechanism. The equilibrium sorption isotherm is very important in design of sorption system. Therefore for finding out the sorption isotherm, the experimental results were analysed by using Freundlich and Langmuir equations. It is seen that, the Freundlich equation is in good agreement with the experimental data. The calcium cation plays an important role in the sorption process.

The results of XRD analysis, pH_{PZC} and pH_{Final} values indicated that ion exchange and dissolution/precipitation mechanisms predominate for the sorption of zinc on our hydroxyapatite.

Appendix A. Supplementary data

Supplementary data associated with this article can be found, in the online version, at doi:10.1016/j.jhazmat.2010.11.087.

References

[1] S. Khan, Q. Cao, Y.M. Zheng, Y.Z. Huang, Y.G. Zhu, Health risks of heavy metals in contaminated soils and food crops irrigated with wastewater in Beijing China, Environ. Pollut. 152 (2008) 686–692.

[2] K. Peng, Ch. Luo, L. Lou, X. Li, Z. Shen, Bioaccumulation of heavy metals by the aquatic plants *Potamogeton pectinatus L.* and *Potamogeton malaianus Miq.* and their potential use for contamination indicators and in wastewater treatment, Sci. Total. Environ. 392 (2008) 22–29.

[3] S. Nayek, S. Gupta, R.N. Saha, Metal accumulation and its effects in relation to biochemical response of vegetables irrigated with metal contaminated water and wastewater, J. Hazard. Mater. 178 (2010) 588–595.

[4] H.Y. Yoo, H.Y. Lee, W.J. Jeong, Preparation of ion exchanger from waste paper cup and removal characteristics of heavy metal, J. Korean Environ. Sci. 11 (2002) 993–999.

[5] P.R. Puranik, K.M. Paknikar, Biosorption of lead and zinc from solutions using *Streptoverticillium cinnamoneum* waste biomass, J. Biotechnol. 55 (1997) 113–124.

[6] S. Azabou, T. Mechichi, S. Sayadi, Zinc precipitation by heavy-metal tolerant sulfate-reducing bacteria enriched on phosphogypsum as a sulfate source, Miner. Eng. 20 (2007) 173–178.

[7] Z. Hubicki, A. Jakowicz, A. Łodyga, Application of the ion-exchange method to remove metallic ions from waters and sewages, Stud. Surf. Sci. Catal. 120 (1999) 497–531.

[8] M. Mohsen-Nia, P. Montazeri, H. Modarress, Removal of Cu^{2+} and Ni^{2+} from wastewater with a chelating agent and reverse osmosis processes, Desalination 217 (2007) 276–281.

[9] H. Polat, D. Erdogan, Heavy metal removal from waste waters by ion flotation, J. Hazard. Mater. 148 (2007) 267–273.

[10] P. Guillaume, N. Leclerc, F. Lapicque, C. Boulanger, Electroleaching and electrodeposition of zinc in a single-cell process for the treatment of solid waste, J. Hazard. Mater. 152 (2008) 85–92.

[11] G. Vázquez, M. Calvo, M.S. Freire, J. González-Alvarez, G. Antorrena, Chestnut shell as heavy metal adsorbent: optimization study of lead, copper and zinc cations removal, J. Hazard. Mater. 172 (2009) 1402–1414.

[12] A. Hawari, Z. Rawajfih, N. Nsour, Equilibrium and thermodynamic analysis of zinc ions adsorption by olive oil mill solid residues, J. Hazard. Mater. 168 (2009) 1284–1289.

[13] S. Meski, H. Khireddine, S. Ziani, S. Rengaraj, M. Sillanpaa, Comparative study on the removal of zinc(II) by bovine bone billy goat bone and synthetic hydroxyapatite, Desalin. Water Treat. 16 (2010) 271–281.

[14] A. Corami, S. Mignardi, V. Ferrini, Copper and zinc decontamination from single- and binary-metal solutions using hydroxyapatite, J. Hazard. Mater. 146 (2007) 164–170.

[15] K.K.H. Choy, G. McKay, Sorption of cadmium, copper, and zinc ions onto bone char using Crank diffusion model, Chemosphere 60 (2005) 1141–1150.

[16] I.S. Harding, N. Rashid, K.A. Hing, Surface charge and the effect of excess calcium ions on the hydroxyapatite surface, Biomaterials 26 (2005) 6818–6826.

[17] C. Stötzel, F.A. Müller, F. Reinert, F. Niederdraenk, J.E. Barralet, U. Gbureck, Ion adsorption behavior of hydroxyapatite with different crystallinities, Colloids Surf. B 74 (2009) 91–95.

[18] H. Khireddine, S. Saoudi, S. Ziani, S. Meski, S. Meskour, Effect of EDTA (acid and salt) on the formation of hydroxyapatite by sol gel processing: a comparative study, Asian J. Chem. 21 (2009) 3885–3891.

[19] H. Song, E.R. Carraway, Y. Hun Kim, B. Batchelor, B. -Hun Jeon, J.-G. Kim, Amendment of hydroxyapatite in reduction of tetrachloroethylene by zero-valent zinc: Its rate enhancing effect and removal of Zn(II), Chemosphere 73 (2008) 1420–1427.

[20] S. Meski, F. Aissani, H. Khireddine, Modeling of the adsorption of phenol on the commercial activated carbon by experimental design, Int. Rev. Chem. Eng. 1 (2009) 515–519.

[21] O. Lacin, B. Bayrak, O. Korkut, E. Sayan, Modeling of adsorption and ultrasonic desorption of cadmium (II) and zinc (II) on local bentonite, J. Colloid Interface Sci. 292 (2005) 330–335.

[22] E. Şayan, Ultrasound-assisted preparation of activated carbon from alkaline impregnated hazelnut shell: an optimization study on removal of Cu^{2+} from aqueous solution, Chem. Eng. J. 115 (2006) 213–218.

[23] S. Chegrouche, A. Bensmaili, Removal of Ga(III) from aqueous solution by adsorption on activated bentonite using a factorial design, Water Res. 36 (2002) 2898–2904.

[24] J. Goupy, Plans d'esperiences pour surface de réponse, Edition DUNOD Paris, 1999.

[25] G. Sado, M.C. Sado, Les plans d'expériences et l'expérimentation à l'assurance qualité, Edition AFNOR Technique 1991.

[26] E.E. Berry, The structure and composition of some calcium-deficient apatites, J. Inorg. Nucl. Chem. 29 (1967) 317–327.

[27] A. Corami, S. Mignardi, V. Ferrini, Cadmium removal from single- and multi-metal (Cd + Pb + Zn + Cu) solutions by sorption on hydroxyapatite, J. Colloid Interface Sci. 317 (2008) 402–408.

[28] E. Landi, A. Tampieri, G. Celotti, R. Langenati, M. Sandri, S. Sprio, Nucleation of biomimetic apatite in synthetic body fluids: dense and porous scaffold development, Biomaterials 26 (2005) 2835–2845.

[29] D.W. Holcomb, R.A. Young, Thermal decomposition of human tooth enamel, Calcif. Tissue Int. 31 (1980) 189–201.

[30] S. Raynaud, E. Champion, J.P. Lafon, D. Bernache-Assollant, Calcium phosphate apatites with variable Ca/P atomic ratio III. Mechanical properties and degradation in solution of hot pressed ceramics, Biomaterials 23 (2002) 1081–1089.

[31] S.F. Cavalitto, C.F. Mignone, Application of factorial and Doehlert designs for optimization of protopectinase production by a *Geotrichum klebahnii* strain, Process Biochem. 42 (2007) 175–179.

[32] A. Erto, R. Andreozzi, F.Di. Natale, A. Lancia, D. Musmarra, Experimental and statistical analysis of trichloroethylene adsorption onto activated carbon, Chem. Eng. J. 156 (2010) 353–359.

[33] F. Li, A. Yuasa, K. Ebie, Y. Azuma, Microcolumn test and model analysis of activated carbon adsorption of dissolved organic matter after precoagulation: effects of pH and pore size distribution, J. Colloid Interface Sci. 262 (2003) 331–341.

[34] K. Zhang, W.H. Cheung, M. Valix, Roles of physical and chemical properties of activated carbon in the adsorption of lead ions, Chemosphere 60 (2005) 1129–1140.

[35] K. Yetilmezsoy, S. Demirel, R.J. Vanderbei, Response surface modeling of Pb(II) removal from aqueous solution by *Pistacia vera* L.: Box–Behnken experimental design, J. Hazard. Mater. 171 (2009) 551–562.

[36] S. Baillez, A. Nzihou, The kinetics of surface area reduction during isothermal sintering of hydroxyapatite adsorbent, Chem. Eng. J. 98 (2004) 141–152.

[37] S. Baillez, A. Nzihou, D. Bernache-Assolant, E. Champion, P. Sharrock, Removal of aqueous lead ions by hydroxyapatites: equilibria and kinetic processes, J. Hazard. Mater. 139 (2007) 443–446.

[38] J. Li, Y. Li, L. Zhang, Y. Zuo, Composition of calcium deficient Na-containing carbonate hydroxyapatite modified with Cu(II) and Zn(II) ions, Appl. Surf. Sci. 254 (2008) 2844–2850.

[39] Y.S. Ho, G. McKay, Pseudo-second order model for sorption processes, Process Biochem. 34 (1999) 451–465.

[40] S. Meski, S. Ziani, H. Khireddine, Removal of lead ions by hydroxyapatite prepared from eggshell, J. Chem. Ing. Data 55 (2010) 3923–3928.

[41] G. Limousin, J.P. Gaudet, L. Charlet, S. Szenknect, V. Barthès, M. Krimissa, Sorption isotherms: a review on physical bases, modeling and measurement, Appl. Geochem. 22 (2007) 249–275.

[42] S.P. Ramnani, S. Sabharwal, Adsorption behavior of Cr(VI) onto radiation crosslinked chitosan and its possible application for the treatment of wastewater containing Cr(VI), React. Funct. Polym. 66 (2006) 902–909.

[43] L. Wu, W. Forsling, P.W. Schindler, Surface complexation of calcium minerals in aqueous solution: 1. Surface protonation at fluorapatite–water interfaces, J. Colloid Interface Sci. 147 (1991) 178–185.

[44] E. Valsami-Jones, K.V. Ragnarsdottir, A. Putnis, D. Bosbach, A.J. Kemp, G. Cressey, The dissolution of apatite in the presence of aqueous metal cations at pH 2–7, Chem. Geol. 151 (1998) 215–233.

[45] K.P. Sanosh, M.-C. Chu, A. Balakrishnan, Y.-J. Lee, T.N. Kim, S.-J. Cho, Synthesis of nano hydroxyapatite powder that simulate teeth particle morphology and composition, Curr. Appl. Phys. 9 (2009) 1459–1462.

[46] Z.Y. Li, W.M. Lam, C. Yang, B. Xu, G.X. Ni, S.A. Abbah, K.M.C. Cheung, K.D.K. Luk, W.W. Lu, Chemical composition, crystal size and lattice structural changes after incorporation of strontium into biomimetic apatite, Biomaterials 28 (2007) 1452–1460.

[47] F Miyaji, Y. Kono, Y. Suyama, Formation and structure of zinc-substituted calcium hydroxyapatite, Mater. Res. Bull. 40 (2005) 209–220.

[48] A. Bigi, E. Foresti, M. Gandolfi, M. Gazzano, N. Roveri, Inhibiting effect of zinc on hydroxyapatite crystallization, J. Inorg. Biochem. 58 (1995) 49–58.

[49] R.Z. LeGeros, J.P. LeGeros, Dense hydroxyapatite, in: L.L. Henc, J. Wilson (Eds.), An Introduction To Bioceramics, World Scientific Publishing Co. Pt. Ltd, London, Hong Kong, Singapore, 1998, pp. 139–180, Adv. Ser. Ceram. 1.